Radial deformation and its related energy variations of single-walled carbon nanotubes

Weibang Lu and Tsu-Wei Chou*
Department of Mechanical Engineering and Center for Composite Materials, University of Delaware, Newark, Delaware 19716, USA

Byung-Sun Kim
Composite Materials Research Group, Korea Institute of Materials Science, Changwon 641-010, South Korea
(Received 6 December 2010; revised manuscript received 11 January 2011; published 11 April 2011)

The radial deformation of a carbon nanotube (CNT) plays a significant role in affecting its mechanical and electrical behavior. In this study, both atomistic simulations and continuum analysis are adopted to study the structural transformations and their related energy variations during the radial deformation of single-walled CNTs (SWCNTs). It is found that for SWCNTs with radius larger than 1.05 nm, they would collapse under radial deformations. The larger the SWCNT radius, the easier it would collapse. The energy barrier is a negative exponent function of SWCNT radius. For SWCNTs with radius larger than 1.90 nm, the collapsed states are more stable than their undeformed states. These different behaviors are due to the variation of contributions from the bending strain energy and the van der Waals interaction energy between opposite walls of the SWCNT to the total energy. Good agreements are achieved between the results of the atomistic simulation approach and the continuum analysis.

DOI: 10.1103/PhysRevB.83.134113 PACS number(s): 62.25.−g

I. INTRODUCTION

Carbon nanotubes (CNTs) have attracted enormous scientific and technological interest over the past two decades. Extensive experimental and theoretical studies have been made to reveal CNTs' unique physical and mechanical properties. It is now well known that CNTs possess high axial Young's moduli (∼1.0 TPa),[1–3] high axial tensile strength (∼63 GPa),[4] and high axial strain at break (∼40%).[5] Based on these superb axial mechanical properties, many applications of CNTs have been reported in the literature. For example, CNTs can be spun continuously from a CNT carpet to form CNT fibers.[6–10] Comparing with the commercial carbon fibers, the spun CNT fibers possess comparable Young's moduli and strength, but much higher toughness.[8]

Unlike the high stiffness in the axial direction, CNTs are rather flexible when subject to radial deformation. With increasing radial external hydrostatic pressure or indentation forces, CNT cross sections would deform continuously from circular to elliptical to peanutlike configurations.[11–13] For larger-radius CNTs, the peanutlike deformed structure can be transformed to dumbbell-like configurations due to the van der Waals (vdW) attractions between the opposite walls of CNTs, and this structure is energetically stable even when the applied force is unloaded. This stable dumbbell-like CNT is defined as the collapsed CNT.[11,12] The collapse of CNTs increases the contact area between neighboring CNTs in a CNT fiber. The resulting enhancement in intertube load transfer efficiency improves the mechanical properties of CNT fibers.[14,15] Also, the radial deformation of CNTs strongly affects their electrical and optical properties. For instance, radial deformation and collapse can induce semiconductor-metal transition in SWCNTs and double-walled CNTs (DWCNTs).[16,17]

The collapse of CNTs has been extensively studied using experimental methods, atomistic simulations, and continuum mechanics analysis. Chopra *et al.*[18] observed fully collapsed multiwalled CNTs (MWCNTs) through transmission electron microscopy. Elliott *et al.*[19] investigated the collapse of SWCNT bundles under hydrostatic pressure by using both Raman spectroscopy analysis and classical molecular dynamics (MD) simulations. They found that SWCNTs undergo a discontinuous collapse transition under hydrostatic pressure. The transition pressure decreases with increasing nanotube diameter and is independent of the chirality of SWCNTs. Gadagkar *et al.*[20] studied the collapse of SWCNT and DWCNT bundles under hydrostatic pressure using classical MD simulations. Their results showed that the critical pressure of DWCNT is close to the sum of the values obtained for the inner and the outer tubes considered separately as SWCNTs. Liu and co-workers[21,22] studied the collapsed states of single-walled and MWCNTs using the atomic-scale finite element method (AFEM). However, the energy barrier, which is of major physical significance, has not been studied. Tang *et al.*[23] studied the collapse of SWCNTs using continuum analysis and assumed that the collapsed SWCNT is composed of a flat contact zone, a semicircle at each end, and a transition zone connecting them. Zhang *et al.*[12] studied the transition states and minimum energy pathways for the collapse of SWCNTs and DWCNTs using the theory of finite crystal elasticity based on the exponential Cauchy-Born rule.

In this work, we investigate the mechanical and structural properties of SWCNTs under antisymmetrical displacement boundary conditions by using AFEM. Guided by the atomistic simulation results, a continuum model is also developed and analyzed using continuum mechanics approach for studying the radial deformation of SWCNTs. The energy barriers (E_b) of the collapse of SWCNTs are found to be a negative exponent function of the radius (R): $E_b = 3.30R^{-0.76}$(eV/nm). Furthermore, the energy differences between the initial state and collapsed state of SWCNTs are obtained, which also have a simple relationship with SWCNT radius. The results of continuum model agree very well with those of atomistic simulations. The concise, closed-form expressions of both energy variation and energy barrier reported here form the basis for the evaluation and design of nanotube-based microscopic structures, such as continuous nanotube fibers.

II. METHODOLOGY

A. Atomistic simulations

The AFEM[21,24] is adopted in this work to simulate the radial deformation behavior of SWCNTs. This method models each carbon atom as a node, and accurately describes the C–C covalent bonds and C–C noncovalent bonds by the second-generation interatomic potential[25] and Lennard-Jones (L-J) potential,[26] respectively. In the calculation of noncovalent bond interaction energies, interactomic distances below 0.3 nm are excluded so that the accuracy of the covalent interactions is not affected. On the other hand, noncovalent bonds with interatomic distances that are greater than 1.0 nm are also excluded so as to reduce the time consumption without affecting the accuracy of simulations. The total energy of the system is the sum of the energies of all covalent bonds and noncovalent bonds. The total energy is then minimized using both the first- and the second-order derivatives of the energy to determine the positions of carbon atoms. AFEM is a kind of static simulation where the thermo effect is not considered. The computational effort of this method increases linearly with the carbon atom numbers. Therefore, this method is much faster than the classical MD simulations, where the computational effort increases with the square of carbon atom numbers. AFEM has been successfully applied in investigating the properties of carbon systems, such as the hydrogen storage capacity of CNTs[27] and the vibration mode transformation in carbon nanorings and SWCNTs.[28] Researchers have found that the chirality has little effect on the radial deformation of CNTs,[12,19] which means the stacking effect is negligible. This is mainly due to the fact that in the collapse transformation of SWCNTs, the opposite walls of the contact zone seek to form the energetically more favorable AB stacking through translation and rotation between the two walls. Thus, only armchair SWCNTs are studied here.

In our simulations, the lengths of all the SWCNTs are around 10 nm, which is about 40 times of the lattice constant of SWCNTs, and is considered to be long enough to eliminate the boundary effects. Figure 1 shows a relaxed SWCNT(20,20). The relaxed SWCNT is taken as the initial state of the subsequent simulations. The energy densities, denoted by e, of several SWCNTs $(5n,5n)(n = 2–8)$ are shown in Fig. 2 (solid squares). It is noted that the energy density decreases with increasing radius, which is in agreement with previous simulation observations.[29] By adopting the concept that a SWCNT can be considered as formed by rolling up a graphene sheet,[1,3] the energy density of the SWCNT e, can be calculated as $e = D/(2R^2) + e_0$, where D is the bending stiffness of the SWCNT and e_0 is the energy density of a graphene sheet. D and e_0 are obtained as 0.665 eV and 3.45 eV/nm^2, respectively, by linear fitting the energy density data of different SWCNTs obtained from AFEM, as shown in Fig. 2. The bending stiffness so obtained is a little bit smaller than 0.85 eV,[30] which was obtained by using classical MD simulations. This discrepancy may be attributed to the different bond potentials used in these two simulations.

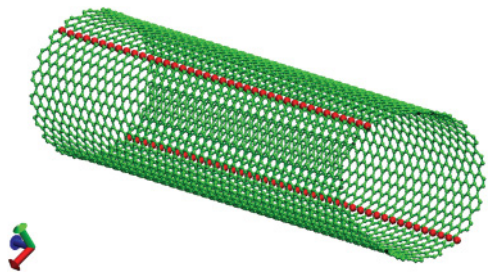

FIG. 1. (Color online) The initial atomic structure of CNT (20,20) with length 10.2 nm. The red atoms are forced to move inward during the radial deformation.

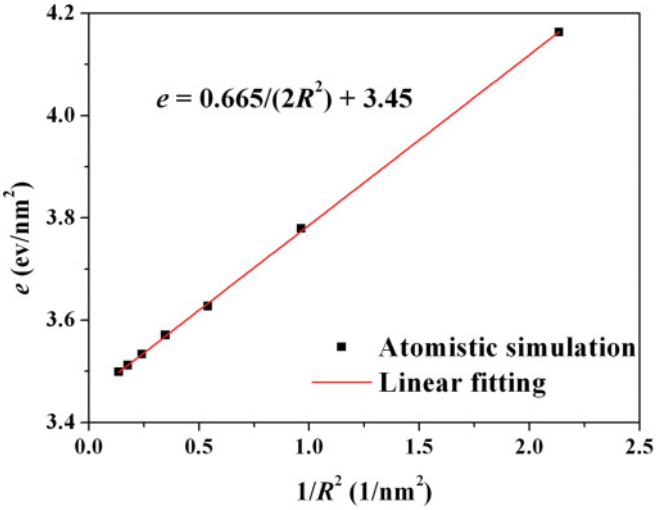

FIG. 2. (Color online) The linear relationship between the strain energy density and $1/R^2$ at the initial state.

To simulate the radial deformation, two lines of atoms on the diametrically opposite walls (as shown in Fig. 1, marked in red) are forced to move toward to the center line of the SWCNT in steps of small increment. The total energy of the SWCNT is obtained from the simulation at each displacement step. Figure 3 shows the radial deformation progression of SWCNT(20,20). It can be clearly seen that with increasing inward displacement or decreasing interwall distance d, the cross-section transforms from circular to elliptical to peanut shape, and finally to dumbbell-like collapsed configurations. This cross-section transformation is similar to that of SWCNTs under hydrostatic pressure simulated by classical MD simulations.[11] The energy variations between the deformed

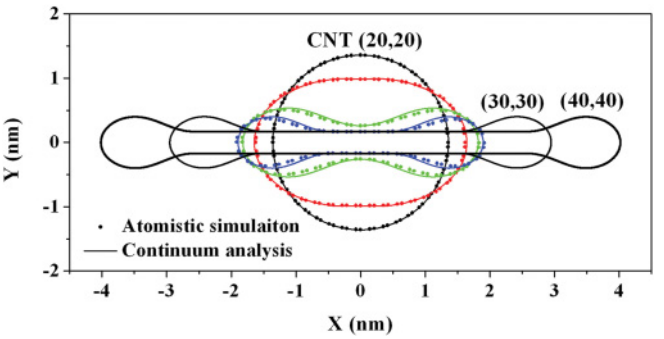

FIG. 3. (Color online) The radial deformation sequence of CNT(20,20) and the cross sections of collapsed CNTs (30,30) and (40,40).

states and the initial state can be readily obtained from the simulation.

B. Continuum mechanics analysis

Although AFEM is much less time consuming than the MD method, it is still difficult to simulate large systems. Continuum mechanics, however, has no such limitation, and has been proved applicable in studying the mechanical properties of CNTs.[30,31] Inspired by cross-section transitions of SWCNTs obtained by atomistic simulations, we put forward a set of continuum models to mimic the radial deformations, as shown in Fig. 4. Based on the consideration that the dominate deformation of the SWCNT is out of plane bending, the wall of the SWCNT is assumed to be inextensible with circumference length of $2\pi R$, where R is the tube radius. So the strain energy only comes from the bending deformation of the cross sections.

At the beginning of the radial deformation, the cross section transforms from circular to elliptical, as represented by an ellipse with parameters a and b [Fig. 4(b)]. The stain energy of a shell under bending can be calculated from $U = \int\int (D\kappa^2/2) dS$, where D and κ are the in-plane bending stiffness and curvature of the shell, respectively.[32] So the strain energy per unit length of the SWCNT is given as

$$U_{\text{ellip}}^{\text{strain}} = \frac{2D}{3a}\left[2\left(1+\frac{a^2}{b^2}\right)E(k_1) - K(k_1)\right], \tag{1}$$

where $k_1 = \sqrt{1-(b/a)^2}$; $E(k_1)$ and $K(k_1)$ are the complete elliptic integral of the first and the second kind, respectively (details of derivation are given in the Appendix). The in-plane bending stiffness D of the SWCNT is taken as 0.665 eV, which is obtained from the AFEM simulations. The circumference of the ellipse is obtained as

$$l = 4aE(k_1). \tag{2}$$

At a given interwall distance $d = 2b$, the energy $U_{\text{ellip}}^{\text{strain}}$ is obtained by minimizing Eq. (1) with respect to parameter a under the condition that the wall is inextensible.

With decreasing interwall distance d, the cross section of the SWCNT is transformed from an ellipse to a peanutlike configuration. Figure 4(c) shows the schematic diagram of the peanutlike cross section, which consists of a semiellipse at each end and two cosine curves connecting the two ends.

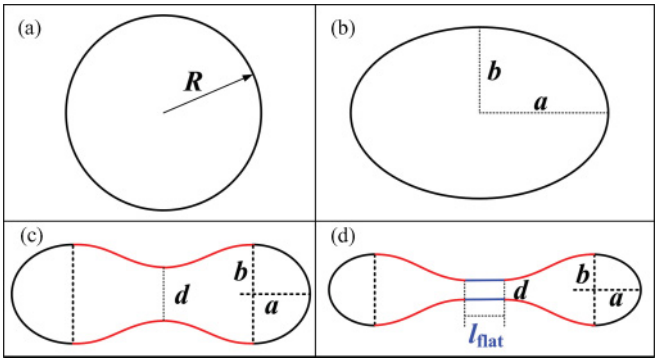

FIG. 4. (Color online) Continuum models for the deformed SWCNTs: (a) initial circular state; (b) ellipse model; (c) peanut model; (d) dumbbell model.

The cosine curves can be obtained by using the continuity conditions at the connecting points. The strain energy per unit length of the SWCNT can be obtained as

$$U_{pn}^{\text{strain}} = \frac{2D}{3a}\left[2\left(1+\frac{a^2}{b^2}\right)E(k_1) - K(k_1)\right] + \frac{4Db}{3a^2k_2}\left[\left(1+k_2^2\right)E(k_2) - \left(1-k_2^2\right)K(k_2)\right], \tag{3}$$

where $k_2 = \sqrt{(1-\frac{d}{2b})/(1-\frac{d}{2b}+2\frac{a^2}{b^2})}$.

The circumference of the cross section is obtained as

$$l = 4aE(k_1) + \frac{8a^2k_2}{b\left(1-k_2^2\right)}E(k_2). \tag{4}$$

Details of derivation are given in the Appendix. At given interwall distance d, the energy U_{pn}^{strain} is obtained by minimizing Eq. (3) with respect to parameters a and b under the condition that the wall is inextensible.

It should be noted that Eq. (3) can only be used when the interwall distance d is larger than the cutoff distance of vdW interactions, which is 1.0 nm in our analysis. When d is less than 1.0 nm, vdW interactions come into play. An explicit expression of the vdW interaction energy between the upper and the lower cosine curves is approximately obtained as the interaction energy between two circles with radius $r = a^2/b$ tangential to the cosine curves, as shown in Fig. 5. The vdW interaction energy between these two circles can be obtained as[29]

$$U_{pn}^{vdW} = \int_d^{\infty} \gamma(y)\sqrt{\frac{R}{y-d}}\,dy, \tag{5}$$

where $\gamma(y)$ is the vdW interaction energy between two graphene sheets of unit area at a spacing y, given as[33]

$$\gamma(y) = 2\pi\rho^2\varepsilon\sigma^2\left(0.4\frac{\sigma^{10}}{d^{10}} - \frac{\sigma^4}{d^4}\right). \tag{6}$$

Here ρ is carbon atom area density of a SWCNT and can be obtained as $\rho = 4/(3\sqrt{3}l_0^2)$, where $l_0 = 0.142$nm is the C–C bond length. ε and σ in Eq. (6) are the Lennard-Jones potential

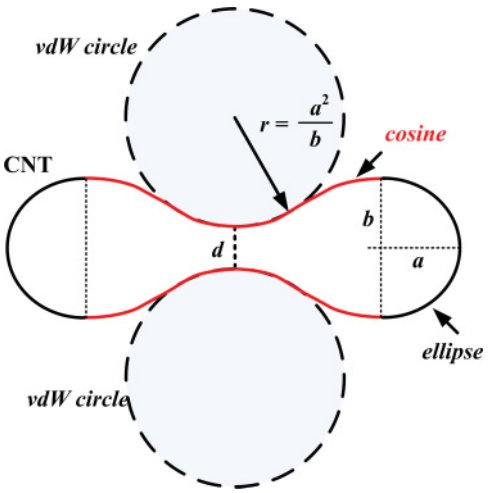

FIG. 5. (Color online) An approximate method for calculating the vdW interactions energy between upper and lower cosine curves.

parameters and they are taken as 0.00239 eV and 0.3415 nm, respectively.[23] From Eqs. (5) and (6), we obtain

$$U_{pn}^{vdW} \approx \pi^2 \rho^2 \varepsilon \sigma^2 a \sqrt{\frac{d}{b}} \left(0.148 \frac{\sigma^{10}}{d^{10}} - 0.625 \frac{\sigma^4}{d^4} \right). \quad (7)$$

So, when the interwall distance d is less than 1.0 nm, the total energy of SWCNT, U_{pn}, is the sum of the strain energy and the vdW interaction energy; that is,

$$U_{pn} = U_{pn}^{\text{strain}} + U_{pn}^{vdW}. \quad (8)$$

At a given interwall distance d, the total energy U_{pn} is minimized with respect to parameters a and b under the condition that the wall is inextensible. Thus, the total energy and the configuration of the deformed cross section can be obtained.

For certain SWCNTs, with further decrease interwall distance d, the cross section would deform to a dumbbell-like configuration due to the interwall vdW interactions. This dumbbell-like cross section is assumed to be composed of a flat contact zone, a semiellipse at each end, and two transition zones connecting the contact zone and the semiellipse, as shown in Fig. 4(d). The transition zones are represented by cosine curves. The total strain energy of the SWCNT U_{pn}^{strain} and the vdW interaction energy U_{pn}^{vdW} of the transition zones can be obtained through Eqs. (3) and (7), respectively. The vdW interaction energy of the flat contact zone can be obtained as

$$U_{\text{flat}} = \gamma l_{\text{flat}}, \quad (9)$$

where γ is the vdW interaction energy between two graphene sheets of unit area at a spacing d and l_{flat} is the length of the flat contact zone, which can be obtained as

$$l_{\text{flat}} = \pi R - 2aE(k_1) - \frac{4ak_2}{b(1-k_2^2)} E(k_2). \quad (10)$$

Then the total energy of the deformed SWCNT can be obtained as

$$U_{db} = U_{pn}^{\text{strain}} + U_{pn}^{vdW} + U_{\text{flat}}. \quad (11)$$

At a given interwall distance d, the total energy is minimized with respect to parameters a and b. Then we can obtain the total energy of the deformed SWCNT and the configuration of the deformed cross section.

III. RESULTS AND DISCUSSIONS

In this study, the radial deformation of armchair SWCNTs with chirality ($5n$,$5n$) (n = 2–8) has been studied using both AFEM simulation and continuum analysis. For SWCNT (10,10) with a radius of 0.69 nm, it is found from the AFEM simulation that with decreasing interwall distance d, the cross section transformed from a circle to an ellipse and finally to a peanutlike configuration, as shown in Fig. 6. The energy of this SWCNT increases monotonically with decreasing interwall distance, as shown in Fig. 7(a). The dumbbell-like cross section is not observed in our simulations. This phenomenon can also be confirmed by the continuum analysis. Minimizing the total energy expression of Eq. (11), we obtain that the contact length

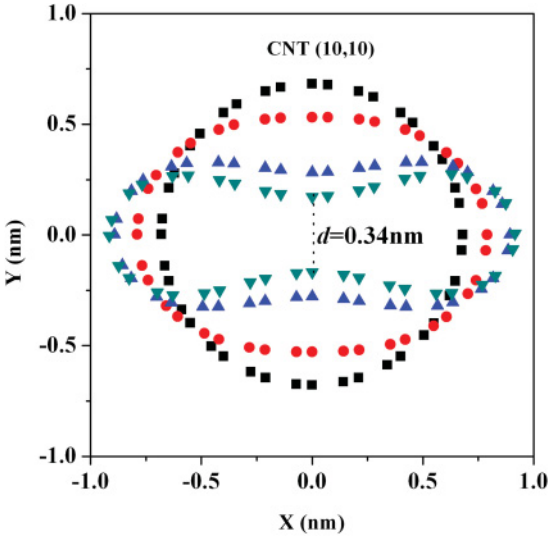

FIG. 6. (Color online) The radial deformation of CNT (10,10) obtained from AFEM simulations. This CNT would not collapse even when the interwall distance is near 0.34 nm.

l_{flat} of –1.16 nm, which is obviously physically unreasonable. This is due to the fact that the interwall vdW interaction energy is not large enough to overcome the bending strain energy to form a flat contact zone. On the other hand, simulations show that if the imposed displacement is removed, the cross section of a SWCNT (10,10) would bounce back to its initial circular state.

For SWCNTs ($5n$,$5n$) and $n \geqslant 3$, the simulations show that the total energy increases initially during the ellipse and peanutlike states and then decreases at certain interwall distance, which is termed as the transition distance. The decrease of energy is due to the fact that the interwall vdW interaction energy increment is larger than the bending strain energy increment. The dots in Fig. 7(a) show the energy variations (relative to the initial circular state) of SWCNTs (20,20), (30,30), and (40,40) during the radial deformation obtained from AFEM simulations. The transition distances of these three SWCNTs are d = 0.51, 0.62, and 0.72 nm, respectively. Beyond the transition states, the imposed displacement is removed and the SWCNTs deform further under the interwall vdW interactions. Finally, the SWCNT collapses when the dumbbell-like cross section is formed, and the interwall spacing within the flat contact zone is around 0.34 nm, which is the interlayer separation of graphite.[4] The radial deformations of zigzag CNT (35,0) and CNT (70,0) with diameters almost the same as those of CNT(20,20) and CNT(40,40), respectively, have also been studied using AFEM. It has been found that the energy variation curves almost coincide for armchair and zigzag CNTs with similar diameters, as shown in Fig. 7(b). The results suggest that the stacking effect is negligible.

The lines in Fig. 7(a) also depict the energy variation of those three SWCNTs obtained from continuum analysis. It is noted that in the early stage of radial deformation, the ellipse deformation model is energetically favorable, and then the peanutlike deformation model becomes energetically more favorable over the ellipse model. When the two opposite

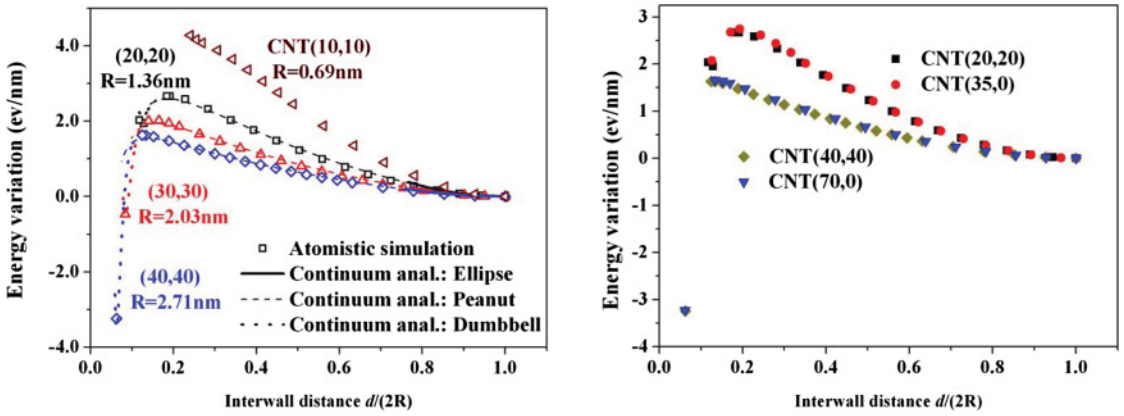

(a) (b)

FIG. 7. (Color online) (a) The energy variation of CNTs with different radius during the radial deformation. (b) Comparison of energy variations of armchair and zigzag CNTs with similar diameters.

walls get close enough, the dumbbell deformation model becomes energetically favorable. The results of the continuum analysis agree well with those from the AFEM simulations. Furthermore, for SWCNTs with radius less than 1.05 nm, the energy of the deformed SWCNT increases monotonically with decreasing interwall distance d, and it would not collapse by transforming to the dumbbell-like configuration.

From the energy variation curves [Fig. 7(a)], it can be concluded that to obtain a collapsed SWCNT, the energy barrier E_b, which is defined as the energy variation at the transition point, should be overcome. Figure 8 shows both the energy barriers and the transition distances of SWCNTs $(5n,5n)$ for $n = 3$–8. It is noted that the energy barrier decreases while the transition distance increases with increasing SWCNT radius. This implies that SWCNTs with larger radius are easier to collapse. The relationship between the energy barrier E_b and SWCNT radius R in Fig. 8 can be fitted by

$$E_b = 3.30R^{-0.76}(\text{eV/nm}). \tag{12}$$

Equation (12) gives a simple explicit formula for predicting the energy barrier that needs to be overcome to obtain a collapsed SWCNT from its initial circular state.

The energy difference, E_d, which is defined as the energy variation at the collapsed (dumbbell-like) state is obtained and shown in Fig. 9. It is noted that for SWCNTs with radius R less than 1.90 nm, such as (15,15), (20,20), and (25,25), the energy difference is always positive, which means that the collapsed state is a metastable state. However, for SWCNTs with radius R larger than 1.90 nm, such as (30,30), (35,35), and (40,40), the energy difference is negative, and the collapsed state is energetically more stable than its circular state. So it can be concluded from the results of calculation that when $R < 1.05$ nm the circular state is energetically favorable; for 1.05 nm $< R <$ 1.90 nm the collapsed state is metastable; and for $R >$ 1.90 nm the collapsed state is energetically favorable.

It is interesting to note that the parameters a and b are constant for all collapsed SWCNTs with different radii, and it is found that a and b are 0.578 and 0.434 nm, respectively. This means that the difference between collapsed SWCNTs with different radii is in the length of the flat contact zone. Thus, the two semiellipse ends, the transition zone between

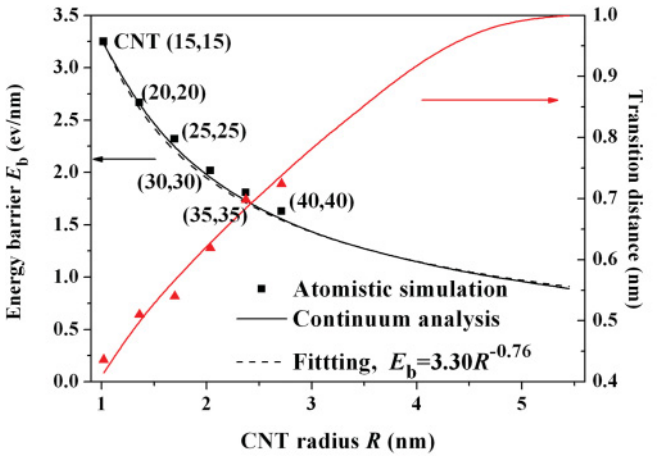

FIG. 8. (Color online) The energy barrier and transition distance of different CNTs under radial deformation.

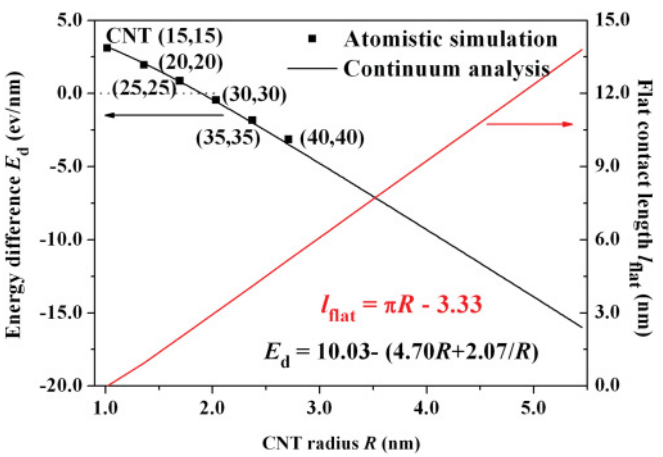

FIG. 9. (Color online) The energy difference and flat contact length of CNTs with different radius.

the ends and the flat contact zone, are identical, as shown in Fig. 3 for the cases of SWCNT(20,20), (30,30), and (40,40). The total length of the nonflat zone is obtained as 6.66 nm, so the length of the flat zone can be obtained as

$$l_{\text{flat}} = (\pi R - 3.33)\,(\text{nm}). \tag{13}$$

The bending strain energy of the collapsed SWCNT is obtained as 5.04 eV/nm, while the vdW interaction energy between the transition zones is obtained as –0.9238 eV/nm. From both atomistic simulation and continuum model analysis, the interwall distance of collapsed SWCNT is around 0.34 nm, which is the same as the equilibrium distance between two parallel graphenes. From Eq. (6), the cohesive energy γ between two unit area graphenes at such distance is obtained as –1.50 eV/nm^2. So the total energy difference of SWCNT with radius R can be expressed as

$$E_d = \left[10.03 - \left(4.70R + \frac{2.07}{R}\right)\right](\text{eV/nm}). \tag{14}$$

IV. CONCLUSIONS

The radial deformation of SWCNTs has a significant effect on their mechanical and physical properties. In this paper, both atomistic simulation and continuum theoretical analysis have been performed to reveal the cross-sectional transformation of SWCNTs during radial deformation. It is found that there exist two critical radii R_1 and R_2, which are 1.05 and 1.90 nm, respectively. For SWCNTs with radius less than R_1, the initial circular states are found to be most stable; for SWCNTs with the radius between R_1 and R_2, the collapsed states are metastable, but the circular states are energetically favorable; and for SWCNTs with radius larger than R_2, the fully collapsed state becomes energetically favorable. The continuum models, termed ellipse, peanut, and dumbbell models, can describe the radial deformation processes very well. The cross sections of all collapsed SWCNTs are nearly the same except for the length of the flat contact zone.

In this paper, the energy variation during the radial deformation has also been investigated. The bending strain energy increases with increasing radial deformation (decreasing interwall distance). For SWCNTs with radius less than 1.05 nm, the total energy of the deformed SWCNTs increases monotonically with interwall distance. For SWCNTs with larger radius, the total energy increases initially until reaching to the critical energy level, termed the energy barrier, and then decreases until the SWCNT totally collapses. The energy barrier for the collapse of SWCNTs decreases with increasing SWCNT radius, and their relationship is represented by a simple formula. The relationship between the energy difference (the energy variation between the collapsed state and the initial circular state) and SWCNT radius is also obtained and represented by a simple expression.

This paper provides a detailed discussion of the radial deformation of SWCNTs, which is useful for understanding the deformations of SWCNTs in general. The methods used in this paper are applicable to investigating the radial deformation mechanism of DWCNTs and MWCNTs, as well as the load transferring mechanism in CNT-based fibers.[9]

V. ACKNOWLEDGMENTS

We acknowledge helpful discussions with Fei Deng. This work is funded by the Army Research Office (Bruce LaMattina, Program Director) and the Korea Foundation for International Cooperation of Science and Technology through a grant provided by the Korean Ministry of Education, Science, and Technology.

APPENDIX : THE STRAIN ENERGY OF DEFORMED SWCNTs BASED ON THE CONTINUUM MODELS

A. Ellipse model

As shown in Fig. 10(a), a quarter of the ellipse can be described by $x = a\sin\alpha$ and $y = b\cos\alpha$, where a and b are the major and minor radius of the ellipse, and α ranges from 0 to $\pi/2$. The first derivative of y with respect to x is $y' = \tan\theta = -\frac{b}{a}\tan\alpha$, where θ represents the slope of the curve, which ranges from 0 to $-\pi/2$. The curvature of the ellipse can then be obtained as $\frac{d\theta}{ds} = -\frac{b}{a\Delta^2}\frac{d\alpha}{ds}$, where $\Delta = \sqrt{1 - k_1^2\sin^2\alpha}$ and $k_1 = \sqrt{1 - \frac{b^2}{a^2}}$. The differential of the arc length is $ds = \sqrt{(\frac{dx}{d\alpha})^2 + (\frac{dy}{d\alpha})^2}d\alpha = a\Delta d\alpha$, which gives that $\frac{d\alpha}{ds} = \frac{1}{a\Delta}$. So The curvature can be rewritten as $\frac{d\theta}{ds} = -\frac{b}{a^2\Delta^3}$.

The length of a quarter of the ellipse is obtained as $l_{\text{quarter}} = \int_0^{l_{\text{quarter}}} ds = \int_0^{\frac{\pi}{2}} a\Delta d\alpha = aE(k_1)$, where $E(k_1) = \int_0^{\frac{\pi}{2}} \sqrt{1 - k_1^2\sin^2\alpha}d\alpha$ is the complete elliptic integral of the second kind. So the length of the SWCNT cross section can be obtained as

$$l = 4\int_0^{l_{\text{quarter}}} ds = 4aE(k_1). \tag{A1}$$

The curvature can be rewritten as $\frac{d\theta}{ds} = -\frac{b}{a^2\Delta^3}$. The bending moment at any point of the curve is then given as

$$M_{\text{oval}}(s) = -D\frac{d\theta}{ds} = D\frac{b}{a^2}\frac{1}{\Delta^3}. \tag{A2}$$

The bending strain energy of this region can be derived as

$$\begin{aligned} E_{\text{quarter}} &= \int_0^{l_{\text{quarter}}} \frac{[M_{\text{oval}}(s)]^2}{2D}ds \\ &= \frac{D}{6a}\left[\frac{2(a^2+b^2)}{b^2}E(k_1) - K(k_1)\right], \end{aligned} \tag{A3}$$

where $K(k_1) = \int_0^{\frac{\pi}{2}} 1/\sqrt{1 - k_1^2\sin^2\alpha}\,\text{d}\alpha$ is the complete elliptic integral of the first kind.

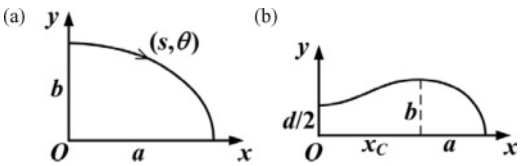

FIG. 10. The coordinate systems of (a) ellipse and (b) peanut models.

The bending strain energy of the hole ellipse can be obtained as

$$U_{\text{oval}} = \frac{2D}{3a}\left[\frac{2(a^2+b^2)}{b^2}E(k_1) - K(k_1)\right]. \quad \text{(A4)}$$

B. Peanut model

Figure 10(b) shows a quarter of the peanut model. The bending strain energy of the two semiellipse ends can also be obtained by Eq. (A4).

The connecting zone is described by a cosine function as $y = -A\cos(wx) + B$, where A and w are constants. Considering the boundary conditions that $y = \frac{d}{2}, y' = 0$ at $x = 0$ and $y = b$, $y' = 0$ at $x = x_C$, where x_C is the projected length of the cosine curve on the x axis and will be determined as a function of a, b and d, we obtain that $A = \frac{b}{2} - \frac{d}{4}$, $B = \frac{b}{2} + \frac{d}{4}$, and $wx_C = \pi$.

The curvature of this region can be expressed as $\frac{d\theta}{ds} = \frac{Aw^2\cos(wx)}{\sqrt{[1+A^2w^2\sin^2(wx)]^3}}$, and the bending moment of any point in this region is given as

$$M_{\text{cosine}}(s) = -D\frac{d\theta}{ds} = -D\frac{Aw^2\cos(wx)}{\sqrt{[1+A^2w^2\sin^2(wx)]^3}}. \quad \text{(A5)}$$

Considering the bending moment continunity condition at the connecting point of the cosine curve and the ellipse, we obtain $w^2 = \frac{b}{a^2}$. So the parameters w and x_C can be obtained as $w = \frac{1}{a}\sqrt{\frac{b}{A}}$ and $x_C = \frac{\pi}{w}$.

Then the bending energy of this region is derived as

$$E_{\text{cosine}} = \int_0^{l_{\text{cosine}}} \frac{[M_{\text{cosine}}(s)]^2}{2D} ds = \frac{Db}{3a^2k_2}\left[\left(1+k_2^2\right)E(k_2) - \left(1-k_2^2\right)K(k_2)\right], \quad \text{(A6)}$$

where $k_2 = \sqrt{(1-\frac{d}{2b})/(1-\frac{d}{2b}+2\frac{a^2}{b^2})}$. The bending strain energy of the peanutlike SWCNT is the sum of the bending energies of two semiellipse ends and the connecting zone; that is,

$$U_{pn}^{\text{strain}} = \frac{2D}{3a}\left[\frac{2(a^2+b^2)}{b^2}E(k_1) - K(k_1)\right] + \frac{Db}{3a^2k_2}\left[\left(1+k_2^2\right)E(k_2) - \left(1-k_2^2\right)K(k_2)\right]. \quad \text{(A7)}$$

The length of the cosine curve is then obtained as $l_{\text{cosine}} = \int_0^{l_{\text{cosine}}} ds = \frac{2a^2k_2}{b(1-k_2^2)}E(k_2)$. So the length of the SWCNT cross section is

$$l = 4aE(k_1) + \frac{8a^2k_2}{b\left(1-k_2^2\right)}E(k_2). \quad \text{(A8)}$$

*chou@udel.edu

[1] D. Sanchez-Portal, E. Artacho, J. M. Soler, A. Rubio, and P. Ordejor, Phys. Rev. B **59**, 12678 (1999).

[2] P. Poncharal, Z. L. Wang, D. Ugarte, and W. A. de Heer, Science **283**, 1513 (1999).

[3] C. Y. Li and T. W. Chou, Int. J. Solids Struct. **40**, 2487 (2003).

[4] M. F. Yu, O. Lourie, M. J. Dyer, K. Moloni, T. E. Kelly, and R. S. Ruoff, Science **287**, 637 (2000).

[5] B. I. Yakobson, M. P. Campbell, C. J. Brabec, and J. Bernholc, Comupt. Mater. Sci. **8**, 341 (1997).

[6] M. Zhang, K. R. Atkinson, and R. H. Baugman, Science **306**, 1358 (2004).

[7] X. B. Zhang, K. L. Jiang, C. Feng, P. Liu, L. N. Zhang, J. Kong, T. H. Zhang, Q. Q. Li, and S. S. Fan, Adv. Mater. **18**, 1505 (2006).

[8] X. F. Zhang, Q. W. Li, T. G. Holesinger, P. N. Arendt, J. Y. Huang, P. D. Kirven, T. G. Clapp, R. F. Depaula, X. H. Liao, Y. H. Zhao, L. X. Zheng, D. E. Peterson, and Y. T. Zhu, Adv. Mater. **19**, 4198 (2007).

[9] T. W. Chou, L. M. Gao, E. T. Thostenson, Z. G. Zhang, and J. H. Byun, Compos. Sci. Technol. **70**, 1 (2009).

[10] W. B. Lu and T. W. Chou, J. Mech. Phys. Solids **59**, 511 (2011).

[11] J. Zang, A. Treibergs, Y. Han, and F. Liu, Phys. Rev. Lett. **92**, 105501 (2004).

[12] S. L. Zhang, R. Khare, T. Belytschko, K. J. Hsia, S. L. Mielke, and G. C. Schatz, Phys. Rev. B **73**, 075423 (2006).

[13] C. J. Park, Y. H. Kim, and K. J. Chang, Phys. Rev. B **60**, 10656 (1999).

[14] K. Koziol, J. Vilatela, A. Moisala, M. Motta, P. Cunniff, M. Sennett, and A. Windle, Science **318**, 1892 (2007).

[15] J. N. Zhao, X. H. Zhang, J. T. Di, G. Xu, X. J. Yang, X. Y. Liu, Z. Z. Yong, M. H. Chen, and Q. W. Li, Small **6**, 2612 (2010).

[16] A. P. M. Barboza, A. P. Gomes, B. S. Archanjo, P. T. Araujo, A. Jorio, A. S. Ferlauto, M. S. C. Mazzoni, H. Chacham, and B. R. A. Neves, Phys. Rev. Lett. **100**, 256804 (2008).

[17] C. E. Giusse, Y. Tison, and S. R. Silva, Nano Lett. **8**, 3350 (2008).

[18] N. G. Chopra, L. X. Benedict, V. H. Crespi, M. L. Cohen, S. G. Louie, and A. Zettl, Nature (London) **377**, 135 (1995).

[19] J. A. Elliot, J. K. W. Sandler, A. H. Windle, R. J. Yong, and M. S. P. Shaffer, Phys. Rev. Lett. **92**, 095501 (2004).

[20] V. Gadagkar, P. K. Maiti, Y. Lansac, A. Jagota, and A. K. Sood, Phys. Rev. B **73**, 085402 (2006).

[21] B. Liu, M. F. Yu, and Y. Huang, Phys. Rev. B **70**, 161402 (2004).

[22] J. Xiao, B. Liu, Y. Huang, J. Zuo, K. C. Hwang, and M. F. Yu, Nanotechnology **18**, 395703 (2007).

[23] T. Tang, A. Jagota, C. Y. Hui, and N. J. Glassmaker, J. Appl. Phys. **97**, 074310 (2005).

[24] B. Liu, Y. Huang, H. Jiang, S. Qu, and K. C. Hwang, Comput. Methods Appl. Mech. Eng. **193**, 1849 (2004).

[25] D. W. Brenner, O. A. Shenderova, J. A. Harrison, S. J. Stuart, B. Ni, and S. Sinnott, J. Phys.: Condens. Matter **14**, 783 (2002).

[26]L. A. Girifalco, M. Hodak, and R. S. Lee, Phys. Rev. B **62**, 13104 (2002).
[27]Y. L. Chen, B. Liu, J. Wu, Y. Huang, H. Jiang, and K. C. Hwang, J. Mech. Phys. Solids **56**, 3224 (2008).
[28]M. X. Shi, Q. M. Li, B. Liu, X. Q. Feng, and Y. Huang, Int. J. Solid Struct. **46**, 4342 (2009).
[29]T. Tang, A. Jagota, and C. Y. Hui, J. Appl. Phys. **97**, 074304 (2005).
[30]B. I. Yakobson, C. J. Brabec, and J. Bernholc, Phys. Rev. Lett. **76**, 2511 (1996).
[31]C. Q. Ru, Phys. Rev. B **62**, 9973 (2000).
[32]L. D. Landau and E. M. Lifshiz, *Theory of Elasticity* (Pergamon, Oxford, 1986).
[33]W. B. Lu, J. Wu, L. Y. Jiang, and Y. Huang, Philos. Mag. **87**, 2221 (2007).